Talanta 103 (2013) 130–136

Contents lists available at SciVerse ScienceDirect

Talanta

journal homepage: www.elsevier.com/locate/talanta

Fast detection and visualization of minced lamb meat adulteration using NIR hyperspectral imaging and multivariate image analysis

Mohammed Kamruzzaman [a], Da-Wen Sun [a,*], Gamal ElMasry [a], Paul Allen [b]

[a] Food Refrigeration and Computerised Food Technology (FRCFT), School of Biosystems Engineering, University College Dublin, National University of Ireland, Agriculture and Food Science Centre, Belfield, Dublin 4, Ireland
[b] Ashtown Food Research Centre (AFRC), Teagasc, Dublin 15, Ireland

ARTICLE INFO

Article history:
Received 8 May 2012
Received in revised form
4 October 2012
Accepted 7 October 2012
Available online 11 October 2012

Keywords:
NIR hyperspectral imaging
Adulteration
Authentication
Minced lamb meat
PLSR and MLR

ABSTRACT

Many studies have been carried out in developing non-destructive technologies for predicting meat adulteration, but there is still no endeavor for non-destructive detection and quantification of adulteration in minced lamb meat. The main goal of this study was to develop and optimize a rapid analytical technique based on near-infrared (NIR) hyperspectral imaging to detect the level of adulteration in minced lamb. Initial investigation was carried out using principal component analysis (PCA) to identify the most potential adulterate in minced lamb. Minced lamb meat samples were then adulterated with minced pork in the range 2–40% (w/w) at approximately 2% increments. Spectral data were used to develop a partial least squares regression (PLSR) model to predict the level of adulteration in minced lamb. Good prediction model was obtained using the whole spectral range (910–1700 nm) with a coefficient of determination (R^2_{cv}) of 0.99 and root-mean-square errors estimated by cross validation (RMSECV) of 1.37%. Four important wavelengths (940, 1067, 1144 and 1217 nm) were selected using weighted regression coefficients (Bw) and a multiple linear regression (MLR) model was then established using these important wavelengths to predict adulteration. The MLR model resulted in a coefficient of determination (R^2_{cv}) of 0.98 and RMSECV of 1.45%. The developed MLR model was then applied to each pixel in the image to obtain prediction maps to visualize the distribution of adulteration of the tested samples. The results demonstrated that the laborious and time-consuming tradition analytical techniques could be replaced by spectral data in order to provide rapid, low cost and non-destructive testing technique for adulterate detection in minced lamb meat.

1. Introduction

Meat and meat products are important sources of protein and expensive, therefore new techniques such as novel refrigeration processes [1–11] have been developed to enhance their quality. However attention should also be paid to the safety and authenticity of meat and meat products as they can be attractive targets for adulteration in many ways such as substitution or partial substitution of high value meat by low cost meat or offal or by adding proteins from several origins [12,13]. Therefore the determination of authentication and detection of adulteration are indispensable for the minced meat industry, which is also important for accurate labeling to help consumers to select appropriate types of meat to meet their demands and for traceability as there are consumers who do not accept specific meats in their diet for religious or ethical reasons [14]. A variety of standard analytical methods (chromatography, electrophoretic separation of proteins, immunological procedure and DNA based techniques) are available for the identification and authentication of minced meat, however all of them are slow, invasive and expensive, and also require sophisticated laboratory procedures with monotonous sample preparation, hence not suitable for on-line applications. In essence, methods for these purposes need to be non-destructive, simple, rapid, economic and spatially located [15].

Spectroscopy techniques have successfully been applied as a quick and efficient method for authentication and adulterate detection in minced meat [16–18]. However, single spot conventional spectroscopic technique alone is not able to provide compositional gradients [19–22]. In reality, there are some vital cases where spatial distribution of quality parameters is needed [23], unfortunately only using computer vision techniques [24–29] based on image processing cannot provide the required spectral information. Thus, hyperspectral imaging has been introduced that integrates imaging and spectroscopy in one system to provide both spectral and spatial information from an object. This information then forms a three-dimensional data, which can be analyzed to characterize the object in more detail than imaging or spectroscopy techniques [30]. The power of spectroscopy is used to detect or quantify physical, chemical and biological attributes of the samples based on their spectral signature, and imaging

* Corresponding author. Tel.: +353 1 7167342; fax: +353 1 7167493.
E-mail address: dawen.sun@ucd.ie (D.-W. Sun).
URLS: http://www.ucd.ie/refrig, http://www.ucd.ie/sun (D.-W. Sun).

0039-9140/$ - see front matter © 2012 Elsevier B.V. All rights reserved.
http://dx.doi.org/10.1016/j.talanta.2012.10.020

transforms this information into chemical maps for spatial visualization. As a result, hyperspectral imaging can be used to know what attributes, how much and where they are located in the sample under study [31].

Recently, hyperspectral imaging techniques have received a considerable attention for the quality and safety assessment of meat, and has been successfully implemented for muscles discrimination and prediction of quality attributes in lamb meat [32–34], quality classification of cooked, sliced turkey ham [35], prediction of water holding capacity, pH, color, tenderness and microbial spoilage in beef [36–40], classification, grading and prediction of quality and sensory attributes in pork [41–45], contaminants and tumor detection in chicken [46–49], and assessment of water and fat contents in fish fillets [50]. To the best of our knowledge, there are no research endeavors yet for authentication and adulterate detection in minced meat using hyperspectral imaging.

However, major bottlenecks such as high costs and difficulties in high speed data acquisition and processing have limited the use of this technology in a real time assessment. Nevertheless, hyperspectral imaging technology can be a very useful tool for selecting some important wavelengths for building a multispectral imaging system to meet the speed requirement of industrial production lines [51]. If the high dimensionality of hyperspectral imaging data can be reduced properly by choosing some optimal wavelengths for certain applications, the technology would certainly be incomparable for process monitoring in real-time inspection [23].

Therefore, the development of rapid and reliable methods for authentication and detection of minced meat adulteration is highly desired. Accordingly, a rapid, reliable and more accurate technique based on hyperspectral imaging could be useful for determination of a few key wavelengths to form multispectral system for authentication and adulterate detection in minced meat. Therefore, the main objectives of the current study were:

1. to establish a NIR hyperspectral imaging in the spectral region of 910–1700 nm as a tool for adulterate detection in minced lamb meat;
2. to identify important wavelengths that can be used to design more effective and efficient multispectral real time imaging systems for adulterate detection in minced lamb meat;
3. to develop image processing algorithms for fast and easy detection and visualization of adulteration in spatial domain.

2. Materials and methods

2.1. Preparation of adulterate samples

This study consisted of two parts: the first concerns the identification of the most potential adulterate while the second concerns the detection of adulteration level. The first study was conducted using pure minced lamb meat and lamb meat mixed with a range of potential adulterants including pork, heart, kidney and lung in 20% w/w [16] proportions. Lamb and pork were taken from the shoulder cut. Visible fat was removed from lamb and pork cuts to ensure the highest possible quantity of lean meat in the minced meat. Meat species (i.e. lamb and pork) and offals (i.e. heart, kidney and lung) were cut into small pieces to facilitate mincing. Samples were collected and minced in Teagasc Food Research Centre, Ashtown (Dublin, Ireland) using a laboratory mincer which was carefully washed and dried between preparations. Minced meat was thoroughly mixed with gloved hands. Then, each class was individually vacuum packed and transported to the laboratory of Biosystems Engineering, University College Dublin (UCD) in ice boxes for image acquisition. A total of 200 samples (5 classes $\times$ 40 samples from each class) were prepared, each of 32 g, for the investigation.

The second study was to detect the level of adulteration in minced lamb meat. The lamb samples were adulterated by mixing pork in the range of 2–40% at approximately 2% increments according to weight. Both minced lamb ($\sim$28% fat) and pork ($\sim$15% fat) were purchased from a local supermarket and transported to the laboratory within 30 min. The minced lamb and pork were individually weighed and thoroughly mixed and homogenized to obtain a total sample weight of 32 g. In total 40 samples (two samples per adulterate level) were prepared for the study. For both investigations, the minced meat was put in a circular metal can and imaged using the hyperspectral system.

2.2. NIR hyperspectral imaging system

A laboratory NIR hyperspectral imaging system was used to acquire spectral images of the samples in the reflectance mode. The system consisted of a line-scan spectrograph (ImSpector, N17E, Spectral Imaging Ltd, Finland), a CCD camera with C-mount lens (Xeva 992, Xenics Infrared Solutions, Belgium), an illumination unit of two 500-W tungsten halogen lamps (V-light, Lowel Light Inc, USA), a translation stage (MSA15R-N, AMT-Linearways, SuperSlides & Bushes Corp., India), a data acquisition software (SpectralCube, Spectral Imaging Ltd., Finland). The camera has 320 $\times$ 256 (spatial $\times$ spectral) pixels. The speed of the translation stage was adjusted at 2.8 cm/s to avoid distortion on image size and to provide same spatial resolution (0.578 mm/pixel) in the horizontal and vertical directions in the image. The working spectral range of the system was 890–1750 nm with 256 spectral bands.

2.3. Image acquisition

Each sample was placed on the translation stage and upon entering the FOV of the camera, a hyperspectral subimage of the sample was acquired as line, then the sample/translation stage was moved and another line of spectra was collected. In this way hyperspectral data cube was created from the lines of spectra until spectra from all pixels in the sample were obtained. The acquired hyperspectral image is a three-dimensional (x, y, λ) block of data where the first two dimensions represent for spatial coordinates and the third one is for spectral intensities. The acquired images were stored in a raw format before being processed. The image acquisition process was controlled by the SpectralCube data acquisition software (Spectral Imaging Ltd., Finland). Each image was recorded in the NIR region of 910–1700 nm with a spectral increment of about 3.34 nm between the contiguous bands, thus producing a total of 237 bands.

2.4. Image pre-processing

2.4.1. Hyperspectral images calibration

To obtain the relative reflectance from each image, it was necessary to correct the raw acquired images from the dark current effect of camera using two extra images: dark and standard white references. A white reference (W) image ($\sim$99.9% reflectance) was acquired from a white reference ceramic tile, and a dark reference (D) image ($\sim$0% reflectance) was obtained with the light source off and the camera lens completely covered with its opaque cap. These two reference images were then used to calculate a relative reflectance image (R) of the sample using the following equation:

$$R = (R_0 - D)/(W - D) \quad (1)$$

All steps of image correction were done by utilizing the normalization tool in ENVI 4.6.1 (ITT Visual Information Solutions, Boulder, CO, USA). All the corrected images were then used as the basis for subsequent analysis to extract spectral information, important wavelength selection, prediction, and visualization purposes.

2.4.2. Selection of region of interest

Identifying regions of interest (ROIs) in the tested objects is a very useful task for extracting spectral features. Segmentation could be considered as an essential step to isolate and locate the ROIs. The main intention of the segmentation was to isolate the meat from the background of the sample. In order to separate the minced meat from the image background, a binary mask image was created by subtracting image at 1300 nm (low reflectance) from the image at 940 nm (high reflectance) and the resulting image was segmented using an optimal threshold value of 0.10. Morphological operations were performed on the resultant binary image to remove the isolated parts originated from edges of metal cans and to fill small holes in the mask to produce the final mask used as the main ROI to extract spectral data from the calibrated hyperspectral image.

2.4.3. Extraction of spectral data

The reflectance values of all pixels from a ROI were averaged to obtain only one mean spectrum for each sample. The same procedure was repeated to obtain the spectrum for all hyperspectral images of all tested samples. The extracted spectrum of each sample was then arranged together to form a spectral matrix. In this study, two spectral matrixes were created: one for the identification of the most potential adulterate in minced lamb and another for the detection of level of adulteration in minced lamb. Background segmentation and extraction of spectral data from hyperspectral images were programmed in MatLab (Version 9, The Mathworks Inc., Mass, USA).

2.5. Spectral analysis

2.5.1. Prediction models at full wavelengths

Initial investigation was carried out using PCA to discriminate minced lamb meat from lamb mixed with different potential adulterates and to identify the most potential adulterate by examining clustering of samples according to their spectral variations. PCA transforms spectral data into several principal components (PCs), which are linear combinations of the original spectral data. The first few PCs resulting from PCA retain most of the variation present in all of the original variables. Each PC can be interpreted independently, which permits an overview of the data structure by revealing the relationship between the objects.

PLSR was applied to predict the level of adulteration in minced lamb meat. It is a very popular and effective technique in spectral analysis where predictors (wavelengths) are highly correlated and the number of predictors is much greater than that of observations [52]. The general purpose of PLSR is to find a mathematical relation between two datasets, X (spectra) and Y (level of adulteration). The PLSR compresses the spectral data into orthogonal structures called latent variables (LVs) which describe the maximum covariance between X and Y [53]. Ideally; only the first few LVs carry the overwhelming majority of relevant information in the original variables. The optimum number of LVs should be used to obtain efficient and reliable prediction models and in this study, it was determined at the minimum value of the root mean squared error estimated by leave-one-out cross-validation (RMSECV).

2.5.2. Important wavelengths selection

In this study, weighted regression coefficients (Bw) resulting from the PLSR model were used to select important wavelengths. The wavelengths that correspond to the highest absolute values of regression coefficients were selected as important wavelengths.

2.5.3. Prediction models at important wavelengths

Selected important wavelengths were then used to establish multiple linear regression (MLR) models to predict the level of adulteration. MLR attempts to correlate between two or more explanatory variables and a response variable to produce a linear regression model as:

$$\hat{y} = a_0 + \sum_{i=1}^{k} a_i X_i \quad (2)$$

where X_i ($i=1 \ldots k$) are the independent variables or predictors, k is the number of important wavelengths and a_o and a_i ($i=1 \ldots .k$) are the regression coefficients. All computations and multivariate spectral analyses were carried out using the chemometric software Unscrambler v9.5 (CAMO AS, Trondheim, Norway).

2.5.4. Evaluation of models

The coefficient of determination (R^2), root mean square error of cross-validation (RMSECV) and ratio of percentage deviation (RPD) were used to evaluate the prediction performance of the models. The RPD is calculated as the ratio of standard deviation (SD) of the reference data to the root-mean-square error of cross-validation [54].

2.6. Multivariate image analysis

As each pixel in a hyperspectral image has its own spectrum, the concentration of chemical components can be calculated at each pixel in the sample to generate chemical maps. However, it is practically impossible to measure the precise concentration of composition in every pixel of a sample. Therefore, regression models are used to interpolate these components in all spots of the sample. In this study, the main aim of hyperspectral image processing was to display the hidden information in each pixel in the image to realize the level of adulteration from sample to sample and even within the same sample. This was executed by multiplying between spectrum of each pixel in the image and the regression coefficients obtained from the MLR model based on the selected important wavelengths. Before multiplication, it was imperative to unfold the three dimensional hypercube into a two-dimensional matrix where each row represents the spectrum of a pixel and the columns represent the selected important wavelengths. After multiplication, the resultant vector was folded back to form a 2-D image in which a 5×5 median filter was employed to enhance the visual display. The resulting image is usually called chemical image or prediction map, in which the spatial distribution of the predicted adulteration is easily interpretable. The main steps for creating these prediction maps are depicted in the flowchart shown in Fig. 1. All image processing steps involved in visualization purposes were performed with a program developed using MatLab (Version 9, The Mathworks Inc., Mass, USA).

3. Results and discussion

3.1. Preliminary investigation by PCA

PCA was used to interpret and visualize the spectral data to highlight their properties, groupings, similarities and differences

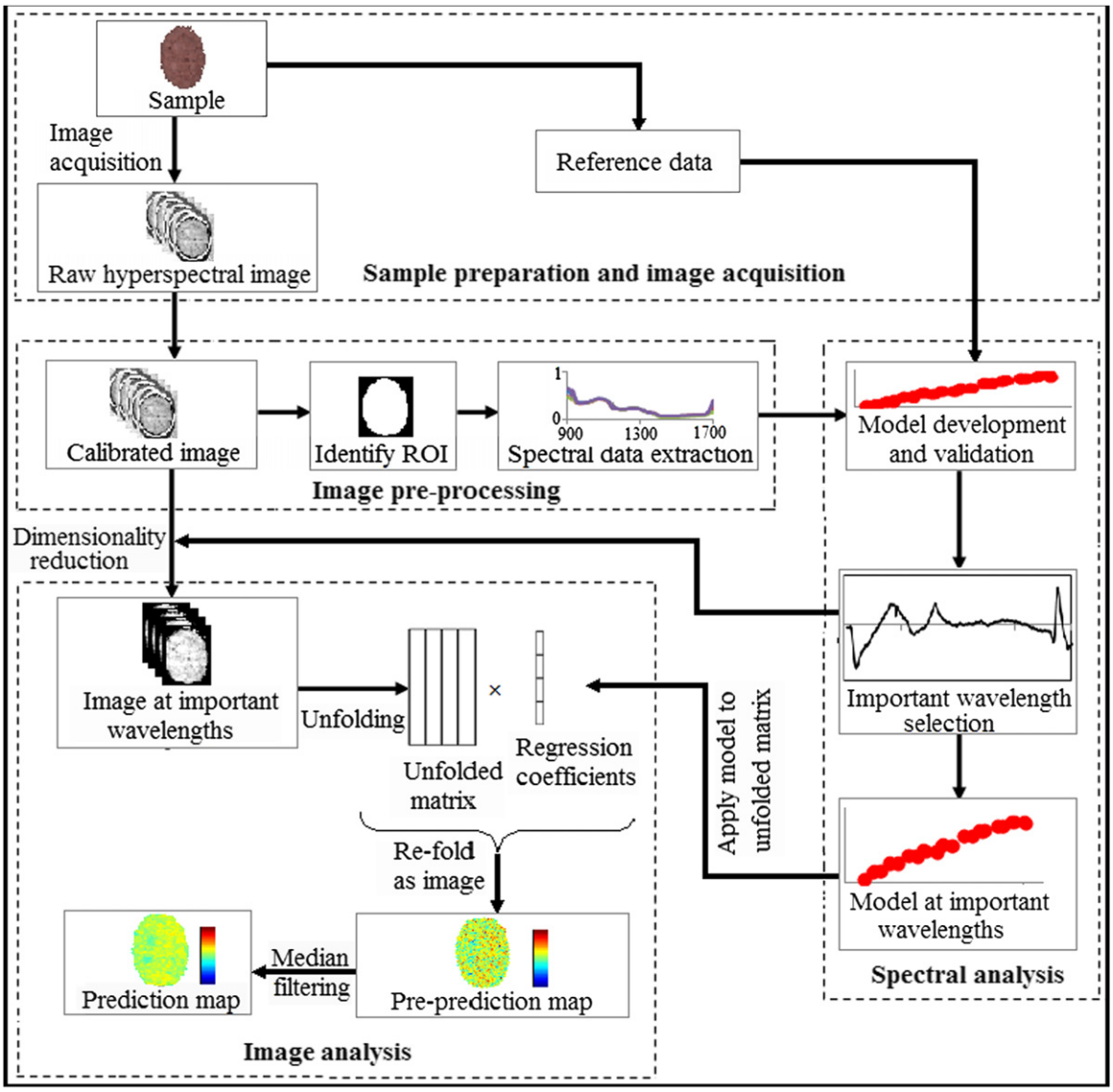

Fig. 1. Flowchart of the main steps for analyzing hyperspectral images and for displaying adulteration in minced lamb samples.

by identifying the most important directions according to spectral features of the tested samples [55]. In essence, when the scores of the principal components are plotted, samples having similar spectral signatures tend to aggregate together or lie close to one another. Generally, the first few principal components resulting from PCA are used to examine the natural pattern among samples and their clustering. The score plot of the first two PCs (explained 95.7% variation) shown in Fig. 2 revealed the clear clustering between pure minced lamb and adulterated minced lamb, where five different clusters were clearly observed without overlap among them. These results imply the possibility of developing analytical method based on hyperspectral imaging for the authentication of minced lamb meat from lamb mixed with potential adulterates. The samples belonging to pure lamb and lamb mixed with 20% pork were clustered much closer to each other followed by lamb mixed with different selected offals. Clearly, Fig. 2 suggested that the most potential adulterate was pork among others since lamb and lamb mixed with pork clustered very closely, indicating that their composition and physicochemical characteristics were quite similar.

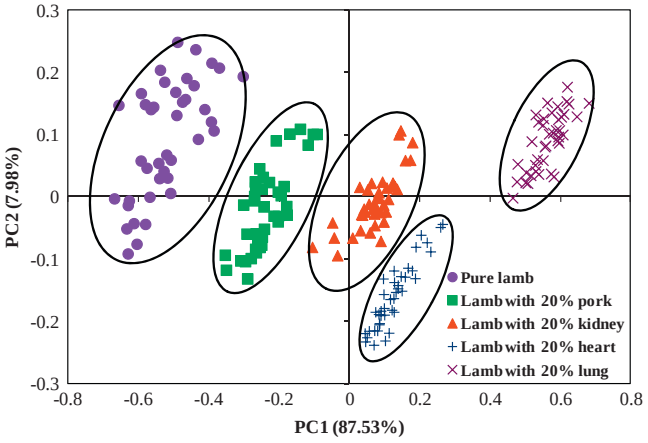

Fig. 2. Scores plot of the first and second principal components of PCA at spectral range of 910–1700 nm for pure lamb and lamb mixed with 20% of different adulterates. Circles shown in the graph do not have any statistical meaning.

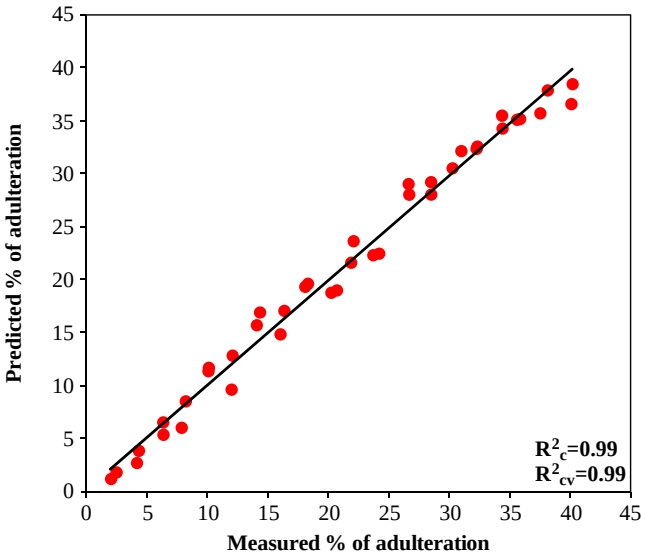

Fig. 3. Predicted versus measured adulteration levels of tested samples using PLSR model at full wavelengths range.

In reality, if the mixture of lamb and pork are predictable then the mixture of lamb and offal would be predicted easily, which needs to be verified in future work. Therefore, the following study will focus only on pure lamb and lamb adulterate with pork for the detection of adulteration level.

3.2. Detection of adulteration level at full wavelengths

The main objective of this investigation was to quantify the level of adulteration in minced lamb. Regression model was developed using PLS to correlate the spectral data with the percentage/level of adulterations. Full cross validation was utilized to validate the calibration model. PLSR prediction results are presented in the scatter plots shown in Fig. 3. It was possible to detect adulteration in minced lamb with high performance in both calibration and cross-validation conditions using five LVs. The level of pork content (adulteration) in minced lamb was predicted with a coefficient of determination in calibration (R^2_c) of 0.99, standard error of calibration (RMSEC) of 1.08%, coefficient of determination in cross-validation (R^2_{cv}) of 0.99 and standard error from cross-validation (RMSECV) of 1.37%. The model had good prediction ability as accentuated by the high values of the coefficients of determination as well as the small difference between RMSEC and RMSECV. These results are very optimistic to indicate the potential hyperspectral imaging as a non-destructive technique for the detection of adulteration in minced meat. Generally, the accuracy (i.e. the closeness between actual and the predicted values) of regression model is considered as excellent when the $R^2 \geq 0.90$ [56]. Therefore, the developed model can be considered sufficiently accurate for future application. The accuracy results found in this study were higher than those reported by Ding and Xu [57] but were similar to those mentioned by Meza-Márquez et al. [17] for predicting adulteration in minced beef using NIR spectroscopy. Meza-Márquez et al. [17] reported R^2_p of 0.99 for predicting adulteration in minced beef mixed with horse meat in the range of 2–90% (w/w), whereas Ding & Xu [58] obtained lower values of R^2 in predicting adulteration in beef hamburgers adulterated with 5–25% (w/w) mutton (R^2_{cv}=0.86) and pork (R^2_{cv}=0.89).

In addition, calibration model was also evaluated based on the RPD. The RPD value of the PLSR model for adulterate detection was 8.51. According to Viscarra Rossel et al. [59], a model is considered to be excellent if the RPD is greater than 2.5. A larger value of RPD indicated greater ability of the model to predict the adulteration precisely in new samples. In this study, the higher RPD value resulted from a wide range of the reference values and/or from smaller RMSECV (1.37%) as compared with the SD (11.66) of the reference values.

3.3. Selection of important wavelengths

The selection of important wavelengths is an essential task to reduce the redundant information in hyperspectral images and to develop an optimized multispectral imaging system for real time applications [52]. When the redundant variables are excluded from the dataset, most of co-linearity problems among variables are alleviated, which ultimately will enhance the model's robustness if the wavelengths which carry most information are selected [35,59]. In our case, the objective was to select the bands that contain the most information about the adulteration in minced lamb. It was done by carrying out correlation using PLSR between spectral data of tested samples and the real concentrations of adulterate levels, where important wavelengths were selected corresponding to the large values (in spite of its sign) of weighted regression coefficients (Bw) resulting from PLSR model. The regression coefficients represent the contributions of spectral variables (i.e. wavelengths) to the calibration model [60]. Seven wavelengths centered at 940, 1067, 1144, 1217, 1635, 1648 and 1685 nm were picked as important wavelengths using Bw plot as shown in Fig. 4. Out of these wavelengths, three wavelengths (1635, 1648 and 1685 nm) in the longer wavelength region were excluded due to high noise associated with these wavelengths. The remaining four wavelengths (940, 1067, 1144 and 1217 nm) were then used as important wavelengths which could later be used to predict the level of adulteration in minced lamb meat. Based on these important wavelengths, it is possible to obtain more robust model and to develop a simple and cost effective multispectral imaging instrument. Once implemented, laborious and time-consuming authentication procedures could be replaced by spectral assay to provide rapid, low cost and non-destructive prediction of adulteration in meat.

As the chemical bonds absorb light energy at specific bands, the selected important wavelengths can be interpreted in terms of the underlying chemical properties of the samples under study. Among the important wavelengths selected (940, 1067, 1144 and 1217 nm), the absorption bands at 940, 1144 and 1217 nm are related to C-H bonds associated with fat [61–63]. This means that the spectral information related to fat absorption bands was important for the prediction of adulteration in minced lamb. This finding might be originated from the differences in fat content among the tested samples. As the degree of adulteration increases,

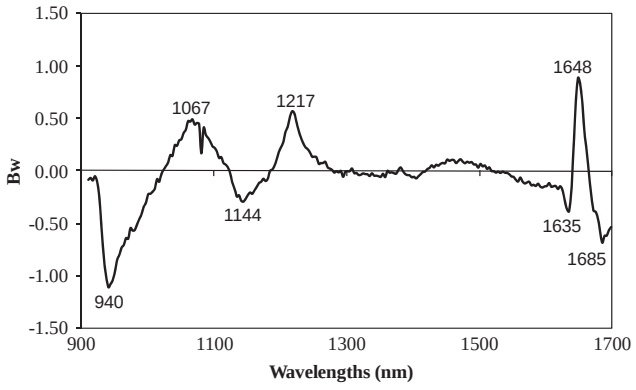

Fig. 4. Weighted regression coefficients of PLSR for selecting important wavelengths.

the fat content of the resultant sample decreases. Because when the minced lamb with high fat content was partially substituted by minced pork with low fat content at 2% increments, the resulted minced had variable fat contents from high (at 2% adulteration) to low (at 40% adulteration). Therefore, it could be concluded that the fat absorption bands were very important in the quantification of pork (adulterate) in minced lamb meat for this particular sample set.

3.4. Detection of adulteration level at reduced wavelengths

Once the important wavelengths were selected, the spectral data were reduced to a matrix N samples × 4 variables by choosing those variables at the selected important wavelengths (940, 1067, 1144 and 1217 nm). MLR model was then built using the reduced spectral data and the results of MLR for predicting adulteration are shown in Table 1. The MLR model had a good performance in predicting adulteration in minced lamb with R_c^2 of 0.99, RMSEC of 1.25%, R_{cv}^2 of 0.98, RMSCV of 1.45% and RPD of 8.04. Additionally, a new PLSR model was also created to verify the potential of selected important wavelengths over the PLSR model developed using the full spectral range. The prediction ability of PLSR model with selected important wavelength was equivalent to the PLSR model with full spectra, with R_{cv}^2 (0.99 *vs.* 0.99), RMSECV (1.42% *vs.* 1.37%) and RPD (8.51 *vs.* 8.21). However, the number of variables needed for prediction was substantially reduced from 237 to 4. Similar prediction results were found between the new PLSR and MLR models; however, the MLR model is simple and easy to interpret than the PLSR models. The following MLR model was obtained which was then applied to spectral images to visualize the distribution of adulteration to demonstrate how the magnitude of adulteration varies from sample to sample even from spot to spot within the same sample:

$$\hat{y} = 29.15 - 356.40 \times \lambda_{940} + 416.51 \times \lambda_{1067} - 177.92 \times \lambda_{1144} + 140.53 \times \lambda_{1293} \quad (3)$$

Table 1
Prediction of adulteration levels using MLR and PLSR at selected important wavelengths (940, 1067, 1144 and 1217 nm).

Models	R_c^2	R_{cv}^2	RMSEC (%)	RMSECV (%)	RPD
MLR	0.99	0.98	1.25	1.45	8.04
PLSR	0.99	0.99	1.27	1.42	8.21

where λ is the reflectance spectral profile with corresponding footnotes indicating the specific wavelengths; $\hat{y}$ is the predicted adulteration level (%).

3.5. Distribution map of adulteration

In contrast to spectroscopy, the major advantage of hyperspectral imaging is the additional information (spatial) involved, which facilitates visualizing the distribution of the components in the tested sample. Since hyperspectral images provide both detailed spectral and spatial information, any complete analysis of such data should include both types of information [64]. Consequently, distribution maps were generated with the aid of multivariate image analysis. The MLR model developed using important wavelengths was applied to each pixel in the spectral image to show the distribution of adulteration in every single spot of the tested sample. In prediction map, variations in adulterate levels were assigned with a linear color scale. Fig. 5 shows prediction maps of some examined samples with their corresponding RGB images. Although it was not possible to recognize the percentage of adulteration in different samples using visual appraisal in their RGB images, the spatial variation of adulteration level between the samples could be easily distinguished in the final prediction maps. The pixel wise prediction maps constructed by multivariate image analysis allowed a rapid and easy interpretation of the hyperspectral data. Although detection of adulteration is a complex task, the results suggest that NIR hyperspectral imaging could become a useful tool for rapid and non-destructive prediction of adulteration in minced meat. Using only four wavelengths a multispectral sensor could be designed for adulterate detection in minced meat. Many researchers successfully used hyperspectral imaging for creating prediction maps of pH, L* value, water holding capacity, fat and fatty acid in beef [36,37,65], pH, L* value and drip loss in pork [43], L* value in lamb [33], and water, fat and salt (NaCl) distribution in fish [50,66,67].

4. Conclusions

The detection of adulteration is attracting an increasing amount of attention for meat processors, researchers and consumers. It is an important issue in the scope of traceability, food

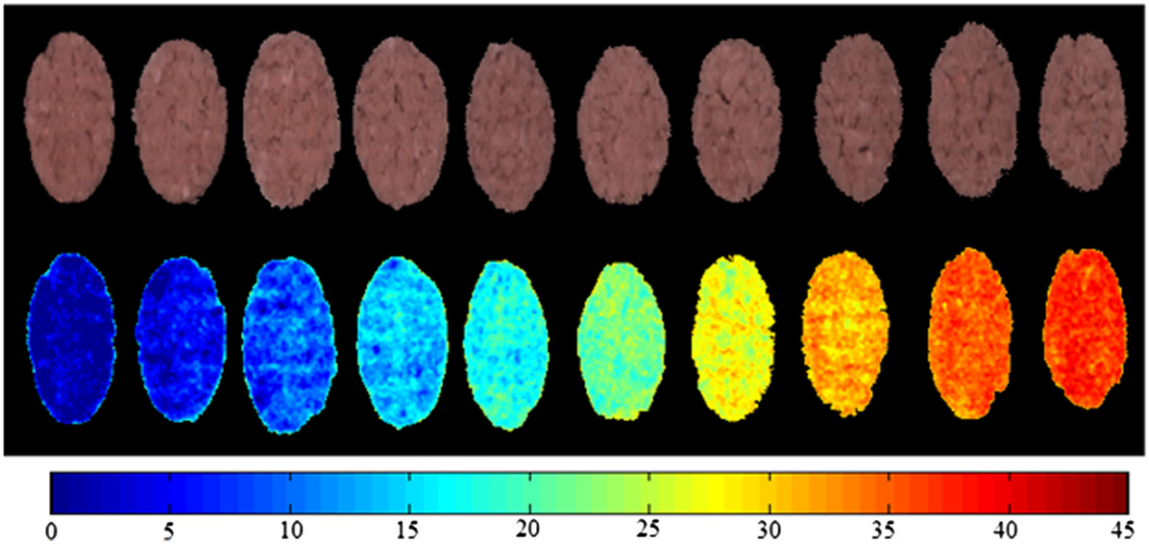

Fig. 5. RGB images (top) and corresponding prediction maps (bottom) of adulteration at different levels from 4% to 40% (left to right) with 4% increments. RGB images were synthesized by combining calibrated hyperspectral images at the wavelengths of 950 nm, 1250 nm and 1300 nm.

safety and quality control. This is the first reported study to use NIR hyperspectral imaging for the detection of adulteration in minced lamb meat. The results demonstrated that the spectral data collected from NIR hyperspectral imaging combined with appropriate multivariate methods could become an interesting tool to detect adulteration in minced lamb meat. The partial least squares regression (PLSR)-based prediction model showed a strong correlation ($R^2_{cv}=0.99$) with adulteration level. Four important wavelengths (940, 1067, 1144 and 1217 nm) were selected to build a MLR model, which yielded a good prediction performance ($R^2_{cv}=0.98$), indicating the potentiality of using hyperspectral imaging to detect adulteration in minced lamb meat. Using these optimum wavelengths, simple, fast and low cost multispectral imaging instrument can be designed for adulterate detection in minced meat. Image processing algorithm was developed to apply the MLR model to each pixel in the image for the distribution of adulteration in all portions of the sample. The spatial concentration mapping provided by hyperspectral imaging is a benefit that cannot be achieved by conventional methods.

Acknowledgments

The authors would like to acknowledge the funding of the Irish Government Department of Agriculture, Fisheries and Food (DAFF) under the Food Institutional Research Measure (FIRM) programme.

References

[1] D.-W. Sun, I.W. Eames, Int. J. of Energy Res. 20 (10) (1996) 871–885, http://dx.doi.org/10.1002/(SICI)1099-114X(199610)20:10<871::AID-ER201>3.3.CO;2-W.
[2] D.-W. Sun, I.W. Eames, S. Aphornratana, Int. J. Refrigeration-Revue Internationale Du Froid 19 (3) (1996) 172–180, http://dx.doi.org/10.1016/0140-7007(96)00010-2.
[3] D.-W. Sun, Energy Convers. Manage. 39 (5–6) (1998) 357–368, http://dx.doi.org/10.1016/S0196-8904(97)00027-7.
[4] D.-W. Sun, Energy Convers. Manage. 40 (8) (1999) 873–884, http://dx.doi.org/10.1016/S0196-8904(98)00151-4.
[5] E.M. Desmond, T.A. Kenny, P. Ward, D.-W. Sun, Meat Sci. 56 (3) (2000) 271–277, http://dx.doi.org/10.1016/S0309-1740(00)00052-8.
[6] K. McDonald, D.-W. Sun, T. Kenny, J. Food Eng. 47 (2) (2001) 139–147, http://dx.doi.org/10.1016/S0260-8774(00)00110-2.
[7] K. Mc Donald, D.-W. Sun, J. Food Eng. 48 (3) (2001) 195–202, http://dx.doi.org/10.1016/S0260-8774(00)00158-8.
[8] L.J. Wang, D.-W. Sun, Int. J. Refrigeration-Revue Internationale Du Froid 25 (7) (2002) 854–861, Article Number: PII S0140-7007(01)00094-9, http://dx.doi.org/10.1016/S0140-7007(01)00094-9.
[9] L.J. Wang, D.-W. Sun, Int. J. Refrigeration-Revue Internationale Du Froid. 25 (7) 2002 862–871, Article Number: PII S0140-7007(01)00095-0, http://dx.doi.org/10.1016/S0140-7007(01)00095-0.
[10] D.-W. Sun, B. Li, J. Food Eng. 57 (4) (2003) 337–345, Article Number: PII S0260-8774(02)00354-0 http://dx.doi.org/10.1016/S0260-8774(02)00354-0.
[11] B. Li, D.-W. Sun, J. Food Eng. 55 (3) (2002) 277–282, Article Number: PII S0260-8774(02)00102-4, http://dx.doi.org/10.1016/S0260-8774(02)00102-4.
[12] D. Cozzolino, I. Murray, LWT—Food Science and Technology 37 (2004) 447–452.
[13] N.Z. Ballin, R. Lametsch, Meat Sci 80 (2008) 151–158.
[14] K. Nakyinsige, Y.B.C. Man, A.Q. Sazili, Meat Sci 91 (2012) 207–214.
[15] L.W. Mamani-Linares, C. Gallo, D. Alomar, Meat Sci 90 (2012) 378–385.
[16] O. Al-Jowder, E. Kemsley, R.H. Wilson, J. Agric. Food Chem. 50 (2002) 1325–1329.
[17] O.G. Meza-Márquez, T. Gallardo-Velázquez, G. Osorio-Revilla, Meat Sci. 86 (2010) 511–519.
[18] A. Rohman Sismindari, Y. Erwanto, Y.B. Che Man, Meat Sci. 88 (2011) 91–95.
[19] F. Liu, Y. He, L. Wang, G. Sun, Food Bioprocess Technol. 4 (2011) 1331–1340.
[20] Y. Liu, R. Gao, Y. Hao, X. Sun, A. Ouyang, Food Bioprocess Technol. 5 (2012) 1106–1112.
[21] Y. Shao, Y. Bao, Y. He, Food Bioprocess Technol. 4 (2011) 1376–1383.
[22] D. Wu, P. Nie, Y. He, Y. Bao, Food Bioprocess Technol. 5 (2012) 1402–1410.
[23] G. ElMasry, D.-W. Sun, CHAPTER 6—Meat quality assessment using a hyperspectral imaging system, Hyperspectral Imaging for Food Quality Analysis and Control, Academic Press, San Diego, 2010, pp. 175-240.
[24] D.-W. Sun, J. Food Eng. 44 (4) (2000) 245–249, http://dx.doi.org/10.1016/S0260-8774(00)00024-8.
[25] T. Brosnan, D.-W. Sun, Comput. Electron. Agric. 36 (2–3) (2002) 193–213, Article Number: PII S0168-1699(02)00101-1, http://dx.doi.org/10.1016/S0168-1699(02)00101-1.
[26] D.-W. Sun, T. Brosnan, J. Food Eng. 57 (1) (2003) 81–89, Article Number: PII S0260-8774(02)00275-3, 10.1016/S0260-8774(02)00275-3.
[27] T. Brosnan, D.-W. Sun, J. Food Eng. 61 (1) (2004) 3–16, http://dx.doi.org/10.1016/S0260-8774(03)00183-3.
[28] C.X. Zheng, D.-W. Sun, L.Y. Zheng, Trends Food Sci. Technol. 17 (12) (2006) 642–655, http://dx.doi.org/10.1016/j.tifs.2006.06.005.
[29] C.X. Zheng, D.-W. Sun, L.Y. Zheng, Trends Food Sci. Technol. 17 (3) (2006) 113–128, http://dx.doi.org/10.1016/j.tifs.2005.11.006.
[30] P. Menesatti, A. Zanella, S. D'Andrea, C. Costa, G. Paglia, F. Pallottino, Food Bioprocess Technol. 2 (2009) 308–314.
[31] P. Menesatti, C. Costa, J. Aguzzi, CHAPTER 8—Quality evaluation of fish by hyperspectral imaging, Hyperspectral Imaging for Food Quality Analysis and Control, Academic Press, San Diego, 2010, pp. 273-294.
[32] M. Kamruzzaman, G. ElMasry, D.-W. Sun, P. Allen, J. Food Eng. 104 (2011) 332–340.
[33] M. Kamruzzaman, G. ElMasry, D.-W. Sun, P. Allen, Anal Chim Acta 714 (2012) 57–67.
[34] M. Kamruzzaman, G. ElMasry, D.-W. Sun, P. Allen, Innov. Food Sci Emerg. Technol. (2012), http://dx.doi.org/10.1016/j.ifset.2012.06.003.
[35] G. ElMasry, A. Iqbal, D.-W. Sun, P. Allen, P. Ward, J. Food Eng. 103 (2011) 333–344.
[36] G. ElMasry, D.-W. Sun, P. Allen, Food Res Int 44 (2011) 2624–2633.
[37] G. ElMasry, D.-W. Sun, P. Allen, J. Food Eng. 110 (2012) 127–140.
[38] G.K. Naganathan, L.M. Grimes, J. Subbiah, C.R. Calkins, A. Samal, G.E. Meyer, Comput. Electron. Agric. 64 (2008) 225–233.
[39] G.K. Naganathan, L.M. Grimes, J. Subbiah, C.R. Calkins, A. Samal, G.E. Meyer, Sens. Instrum. Food Qual. Saf. 2 (2008) 178–188.
[40] Y. Peng, J. Zhang, W. Wang, Y. Li, J. Wu, H. Huang, X. Gao, W. Jiang, J. Food Eng. 102 (2011) 163–169.
[41] J. Qiao, M. Ngadi, N. Wang, A. Gunenc, M. Monroy, C. Gariepy, S. Prasher, Int. J. Food Eng. 3 (2007) 1–12.
[42] D. Barbin, G. Elmasry, D.-W. Sun, P. Allen, Meat Sci. 90 (2011) 259–268.
[43] D.F. Barbin, G. ElMasry, D.-W. Sun, P. Allen, Anal. Chim. Acta. 719 (2012) 30–42.
[44] J. Qiao, M.O. Ngadi, N. Wang, C. Gariepy, S. Prasher, J. Food Eng. 83 (2007) 10–16.
[45] J. Qiao, N. Wang, M. Ngadi, A. Gunenc, M. Monroy, C. Gariepy, S. Prasher, Meat Sci. 76 (2007) 1–8.
[46] S.G. Kong, Y.R. Chen, I. Kim, M.S. Kim, Appl. Opt. 43 (2004) 824–833.
[47] S. Nakariyakul, D.P. Casasent, Opt. Eng. 47 (2008) 087202.
[48] K. Chao, C. Yang, M. Kim, D. Chan, Appl. Eng. Agric. 24 (2008) (2008) 475–485.
[49] B. Park, W. Windham, K. Lawrence, D. Smith, Biosyst. Eng. 96 (2007) 323–333.
[50] G. ElMasry, J.P. Wold, J. Agric. Food Chem. 56 (2008) 7672–7677.
[51] J. Burger, A. Gowen, Chemometr. Intell. Lab. Syst. 108 (2011) 13–22.
[52] M. Taghizadeh, A. Gowen, C.P. O'Donnel, Sens. Instrum. Food Qual. Saf. 3 (2009) 219–226.
[53] P. Menesatti, F. Antonucci, F. Pallottino, G. Roccuzzo, M. Allegra, F. Stagno, F. Intrigliolo, Biosyst. Eng. 105 (2010) 448–454.
[54] F. Antonucci, P. Menesatti, N.M. Holden, E. Canali, S. Giorgi, A. Maienza, S.R. Stazi, Commun. Soil Sci. Plant Anal. 43 (2012) 1401–1411.
[55] J.R. Lucio-Gutiérrez, J. Coello, S. Maspoch, Food Res. Int. 44 (2011) 557–565.
[56] M. Urbano Cuadrado, M.D. Luque de Castro, P.M. Pérez Juan, M.A. Gómez-Nieto, Talanta 66 (2005) 218–224.
[57] H. Ding, R. Xu, J. Agric. Food Chem. 48 (2000) 2193–2198.
[58] R. Viscarra Rossel, H. Taylor, A. McBratney, Eur. J. Soil Sci. 58 (2007) 343–353.
[59] J.P. Wold, T. Jakobsen, L. Krane, J. Food Sci. 61 (1996) 74–77.
[60] P. Ritthiruangdej, R. Ritthiron, H. Shinzawa, Y. Ozaki, Food Chem. 129 (2011) 684–692.
[61] N. Prieto, S. Andrés, F.J. Giraldez, A.R. Mantecon, P. Lavın, Meat Sci. 74 (2006) 487–496.
[62] N. Prieto, R. Roehe, P. Lavín, G. Batten, S. Andrés, Meat Sci. 83 (2009) 175–186.
[63] V. Ortiz-Somovilla, F. Espana-Espana, A.J. Gaitan-Jurado, J. Perez-Aparicio, E.J. De Pedro-Sanz, Food Chem. 101 (2007) 1031–1040.
[64] J. Prats-Montalbán, A. De Juan, A. Ferrer, Chemometr. Intell. Lab. Syst. 107 (2011) 1–23.
[65] K.I. Kobayashi, Y. Matsui, Y. Maebuchi, T. Toyota, S. Nakauchi, J. Near Infrared Spectrosc. 18 (2010) 301–315.
[66] D. Wu, H. Shi, S. Wang, Y. He, Y. Bao, K. Liu, Anal. Chim. Acta 726 (2012) 57–66.
[67] V.H. Segtnan, M. Høy, O. Sørheim, A. Kohler, F. Lundby, J.P. Wold, R. Ofstad, J. Agric. Food Chem. 57 (2009) 1705–1710.